BRAIN COMMUNICATIONS

Oxygenation differs among white matter hyperintensities, intersected fiber tracts and unaffected white matter†

Rikke B. Dalby,[1,2,3] Simon F. Eskildsen,[1] Poul Videbech,[4] Jesper Frandsen,[1] Kim Mouridsen,[1] Leif Sørensen,[3] Peter Jeppesen,[5] Toke Bek,[5] Raben Rosenberg[6] and Leif Østergaard[1,3]

†Preliminary results from this study were accepted for poster presentation at BRAIN & BRAIN PET in Yokohama, Japan, 4–7 July 2019, abstract no. PB03-E04, *Journal of Cerebral Blood Flow and Metabolism* 2019 Jul; 39(Suppl 1): 395.

White matter hyperintensities of presumed vascular origin are frequently observed on magnetic resonance imaging in normal aging. They are typically found in cerebral small vessel disease and suspected culprits in the etiology of complex age- and small vessel disease-related conditions, such as late-onset depression. White matter hyperintensities may interfere with surrounding white matter metabolic demands by disrupting fiber tract integrity. Meanwhile, risk factors for small vessel disease are thought to reduce tissue oxygenation, not only by reducing regional blood supply, but also by impairing capillary function. To address white matter oxygen supply–demand balance, we estimated voxel-wise capillary density as an index of resting white matter metabolism, and combined estimates of blood supply and capillary function to calculate white matter oxygen availability. We conducted a cross-sectional study with structural, perfusion- and diffusion-weighted magnetic resonance imaging in 21 patients with late-onset depression and 21 controls. We outlined white matter hyperintensities and used tractography to identify the tracts they intersect. Perfusion data comprised cerebral blood flow, blood volume, mean transit time and relative transit time heterogeneity—the latter a marker of capillary dysfunction. Based on these, white matter oxygenation was calculated as the steady state cerebral metabolic rate of oxygen under the assumption of normal tissue oxygen tension and vice versa. The number, volume and perfusion characteristics of white matter hyperintensities did not differ significantly between groups. Hemodynamic data showed white matter hyperintensities to have lower blood flow and blood volume, but higher relative transit time heterogeneity, than normal-appearing white matter, resulting in either reduced capillary metabolic rate of oxygen or oxygen tension. Intersected tracts showed significantly lower blood flow, blood volume and capillary metabolic rate of oxygen than normal-appearing white matter. Across groups, lower lesion oxygen tension was associated with higher lesion number and volume. Compared with normal-appearing white matter, tissue oxygenation is significantly reduced in white matter hyperintensities as well as the fiber tracts they intersect, independent of parallel late-onset depression. In white matter hyperintensities, reduced microvascular blood volume and concomitant capillary dysfunction indicate a severe oxygen supply–demand imbalance with hypoxic tissue injury. In intersected fiber tracts, parallel reductions in oxygenation and microvascular blood volume are consistent with adaptations to reduced metabolic demands. We speculate, that aging and vascular risk factors impair white matter hyperintensity perfusion and capillary function to create hypoxic tissue injury, which in turn affect the function and metabolic demands of the white matter tracts they disrupt.

1 Center of Functionally Integrative Neuroscience & MINDLab, Aarhus University Hospital, 8200 Aarhus C., Denmark
2 Centre for Psychiatric Research, Aarhus University Hospital, 8340 Risskov, Denmark
3 Department of Neuroradiology, Aarhus University Hospital, 8200 Aarhus N., Denmark
4 Center for Neuropsychiatric Depression Research, Mental Health Center Glostrup, 2600 Glostrup, Denmark

Received May 5, 2019. Revised August 27, 2019. Accepted October 1, 2019. Advance Access publication November 18, 2019

5 Department of Ophthalmology, Aarhus University Hospital, 8200 Aarhus N., Denmark
6 Centre of Psychiatry Amager, Mental Health Services in the Capital Region of Denmark, 2300 Copenhagen S., Denmark

Correspondence to: Rikke B. Dalby
Department of Neuroradiology,
Aarhus University Hospital,
Palle Juul-Jensens Boulevard 165, J314, 8200 Aarhus N., Denmark
E-mail: rbdalby@dadlnet.dk

Keywords: white matter hyperintensities; MRI; fibertracking; cerebral blood flow; capillary dysfunction

Abbreviations: CBF = cerebral blood flow; CBV = cerebral blood volume; $CMRO_2$ = cerebral metabolic rate of oxygen; CTH = capillary transit time heterogeneity; FLAIR = fluid-attenuated inversion recovery; GRE = gradient echo; MRI = magnetic resonance imaging; MTT = mean transit time; NAWM = normal-appearing white matter; OEF = oxygen extraction fraction; RTH = relative transit time heterogeneity; SE = spin echo; SVD = small vessel disease; WMHs = white matter hyperintensities

Graphical Abstract

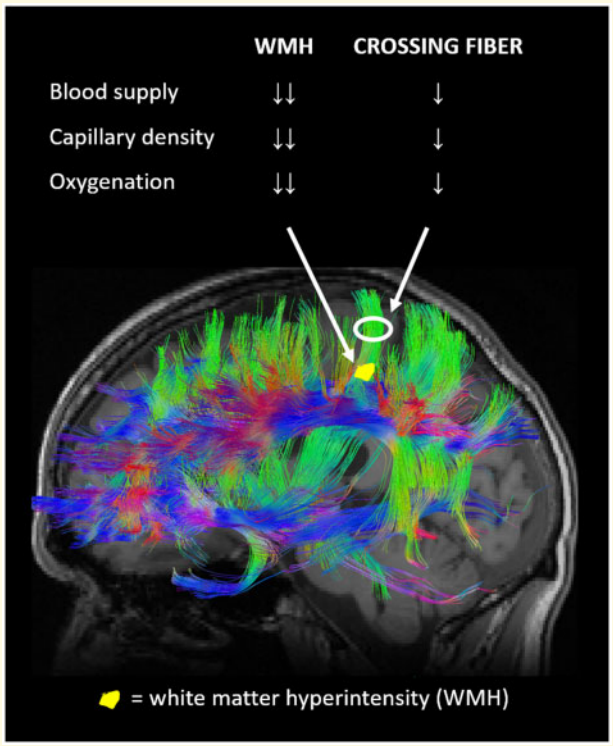

Introduction

Cerebral white matter hyperintensities (WMHs), also known as white matter lesions, are frequent findings on T2-weighted magnetic resonance imaging (MRI) in the elderly, with a reported prevalence of up to ~95% in large population-based studies of people aged 60–65 and older (Longstreth *et al.*, 1996; de Leeuw *et al.*, 2001; Fernando and Ince, 2004). Once considered an incidental finding, increasing evidence over the past decades prove that the presence and extent of WMHs play an important role in cognitive and functional impairment (Pantoni, 2010; Prins and Scheltens, 2015). Higher prevalence of WMHs are associated with increased risk of stroke, dementia, late-life depression and death (Herrmann *et al.*, 2007; Debette and Markus, 2010; van Agtmaal *et al.*, 2017), yet this risk may be modifiable as reflected by the close association between WHMs and vascular risk factors, such as hypertension, diabetes and smoking (Pantoni, 2010). Studies in depression suggest that WMHs are associated with depression severity (Sheline *et al.*, 2010), persistence of cognitive impairment (Kohler *et al.*, 2010), greater risk of subsequent dementia (Steffens *et al.*, 2007) and poor treatment response in the elderly (Hickie *et al.*, 1995; Steffens *et al.*, 2001; Taylor *et al.*, 2003; Chen *et al.*, 2006; Iosifescu *et al.*, 2006).

The pathogenesis of WMHs is complex and not yet fully established—for a comprehensive review, see

(Wardlaw *et al.*, 2013). In general, WMHs are considered a marker of cerebral small vessel disease (SVD) which also entails small subcortical infarcts, lacunes, microbleeds, enlarged perivascular spaces (Virchow–Robin spaces) and brain atrophy (Wardlaw *et al.*, 2013). SVD may result from a range of pathological processes that affect the small arteries, arterioles, capillaries, venules and small veins of the brain (Ostergaard *et al.*, 2016). In particular, the involvement of capillaries are thought to result in disturbed blood brain barrier permeability and transient, repeated episodes of white matter hypoperfusion, perivascular alterations and eventually demyelination, loss of oligodendrocytes and axonal damage (Pantoni and Garcia, 1997; Pantoni, 2010; Iadecola, 2013), which may manifest themselves as WMHs on MRI. However, the association between WMH 'load' (i.e. number and volume) and localization on one hand, and their impact on brain connectivity and function on the other, is still incompletely understood.

The neuroimaging characteristics of WMHs include elevated longitudinal relaxation time (T1) on conventional MRI, reduced magnetization transfer ratio and reduced fractional anisotropy with elevated mean diffusivity and/or apparent diffusion coefficient as observed by diffusion-weighted MRI (Fazekas *et al.*, 2005; Bastin *et al.*, 2009; Dalby *et al.*, 2010*b*; Maniega *et al.*, 2015). These changes reflect demyelination and axonal loss, both in the WMHs themselves and in the surrounding white matter—the latter also referred to as the WMH 'penumbra' (Maillard *et al.*, 2011). Thanks to these methods, altered interstitial fluid mobility has emerged as an early feature in the chain of events that lead to WMHs, as it seemingly precedes demyelination and axonal damage (de Groot *et al.*, 2013; Wardlaw *et al.*, 2015). Perfusion MRI studies have shown reduced cerebral blood flow (CBF) in areas of WMHs (Markus *et al.*, 2000; O'Sullivan *et al.*, 2002), but the interpretation of perfusion data is made difficult by the fact that CBF is closely regulated to meet local metabolic demands, even in disease. As a result, it remains unclear whether tissue damage is the result of CBF reductions, or vice versa (Wardlaw *et al.*, 2015).

In normal brain, both capillary density and resting CBF are closely coupled to local, resting metabolic demands in both grey and white matter (Klein *et al.*, 1986; Borowsky and Collins, 1989). While neurovascular coupling mechanisms adjust CBF according to second-by-second changes in the metabolic demands of brain tissue (Iadecola, 2004), oxygen-sensing mechanisms adapt capillary density according to local metabolic demands in the developing and adult brain (Markham and Greenough, 2004; Zhao *et al.*, 2008). This physiological neurovascular remodelling mechanism includes the activation of hypoxia-inducible factors, but seemingly fails in SVD: Although WMHs reveal histological evidence of hypoxia and upregulated hypoxia-inducible factor levels in human autopsy studies (Fernando *et al.*, 2006), their capillary density, paradoxically, remains low (Brown *et al.*, 2007; Brown and Thore, 2011). Taken together, there is reason to believe that capillary density is uncoupled from either or both CBF and metabolic demands within WMHs and that any effects of WMHs on the metabolism of the fiber tracts they disrupt would lead to a coupled reduction in capillary density and CBF within unaffected, normal-appearing white matter (NAWM).

Until recently, knowledge of CBF, capillary density, and capillary wall oxygen permeability was thought to suffice to infer tissue oxygenation (Renkin, 1985). However, a recent reappraisal of the relation between CBF and tissue oxygenation (Jespersen and Ostergaard, 2012; Angleys *et al.*, 2015; Rasmussen *et al.*, 2015) shows that capillary flow patterns profoundly affect the extraction of oxygen from blood at a given blood supply. Cardiovascular risk factors, such as hypertension, diabetes and low-grade inflammation, can therefore critically reduce the oxygen availability by disturbing capillary flow patterns in terms of increasing the 'shunting' of oxygenated blood though microcirculation. This phenomenon, 'capillary dysfunction' (Ostergaard *et al.*, 2013*a*), has now been implicated in the pathophysiology of dementia (Eskildsen *et al.*, 2017; Nielsen *et al.*, 2017), ischemia (Ostergaard *et al.*, 2015; Engedal *et al.*, 2018) and inherited white matter disease (Lauer *et al.*, 2017) by specialized perfusion MRI tecniques (Mouridsen *et al.*, 2014). Given the evidence of capillary changes in SVD (Ostergaard *et al.*, 2016), we speculate, that capillary dysfunction reduces oxygen availability within WMHs, over and beyond the effects of altered perfusion and capillary density.

We have previously characterized age-related WMHs, intersected white matter tracts, and NAWM as part of a study of WMHs in late-onset depression (Dalby *et al.*, 2010*a*, *b*). In this study cohort, patients and their age- and gender-matched controls show similar WMH load and volume, while patients tend to have 'strategic' WMHs that disrupt fiber tracts connecting regions implicated in cognition and mood regulation. Importantly, across all study participants, MRI indices of white matter molecular and cellular integrity, including the magnetization transfer ratio, apparent diffusion coefficient, and fractional anisotropy of water diffusion, revealed significant differences between WMHs, the white matter tracts they intersect, and NAWM, respectively. We therefore hypothesized, that these microstructural changes would be paralleled by hemodynamic changes across the white matter compartments. Conversely, we did not expect to find depression-related differences in white matter hemodynamics.

Materials and methods

Subjects

The study population is previously described elsewhere (Dalby *et al.*, 2010*a*). In brief, we examined 22 patients

with late-onset first-episode major depression and 22 age- and gender-matched controls with no history of psychiatric illness. All patients fulfilled the criteria for moderate to severe depression according to International Classification of Diseases, 10th revision (ICD-10) (World Health Organization, 1993) and major depression according to Diagnostic and Statistical Manual of Mental Disorders, 4th edition (DSM-IV) (American Psychiatric Association, 2000). We defined late-onset as age 50 years or older at the time of diagnosis. Information on medication, including antidepressants, and vascular risk factors, such as hypertension, hypercholesterolemia, diabetes, cardiovascular disease and smoking (current, past or never) including tobacco years, was collected through clinical interview, medical records, blood samples and electrocardiogram, as previously described (Dalby *et al.*, 2010*a*). We calculated a composite vascular risk factor score and estimated the Framingham 10-year stroke risk, as defined in the Framingham Study (Wolf *et al.*, 1991). All subjects gave written informed consent, and the study was conducted after approval by the regional ethical committee and in accordance with the Declaration of Helsinki (World Medical Association, 2008).

Magnetic resonance imaging

All subjects were scanned on a 3 Tesla GE Signa HDx scanner (GE Medical Systems, Milwaukee, WI, USA). The MRI protocol included 3 D T1-weighted imaging, T2-weighted imaging with a fluid-attenuated inversion recovery (FLAIR) sequence, diffusion-weighted imaging and dynamic susceptibility contrast perfusion-weighted imaging. Results of the diffusion-weighted imaging analyses are described in (Dalby *et al.*, 2010*b*). Perfusion imaging was performed with gradient echo (GRE) and spin echo (SE) echo-planar imaging sequences during a bolus injection of 0.1 and 0.2 mmol/kg contrast media (Gadovist® 1.0 M; Bayer AG, Berlin, Germany) for the GRE and SE echo-planar imaging sequences, respectively. Image acquisition parameters for both sequences comprised slice thickness 5 mm, gap 1.5 mm, 1.88 mm in-plane resolution and TR 1500 ms, while TE was 30 s for GRE and 60 s for SE. The flip angle for GRE was 60°. The contrast bolus was injected after 15 repetitions and immediately followed by injection of 30 ml of physiological saline at a rate of 5 ml/s. A total of 50 repetitions were performed. Bolus injection was delivered in the right antecubital vein for all subjects, except for one patient and two controls where difficult intravenous access required insertion into the left antecubital vein. Total MRI protocol acquisition time was ~50 min.

White matter hyperintensities and tractography

We defined WMHs as hyperintensities on FLAIR images without cavitation (Wardlaw *et al.*, 2013). Subcortical/deep and periventricular WMHs were identified on the FLAIR images by an experienced neuroradiologist (L.S.), blinded to subject status, and were initially graded according to Fazekas' scale (Fazekas *et al.*, 1987), where subcortical/deep WMHs reflect a continuum of increasing severity of tissue damage, depending on lesion size, whereas punctate WMHs are considered of nonischemic origin and mostly confined to widening of perivascular spaces, early confluent and confluent WMHs reflect varying degrees of demyelination, axonal loss and gliosis (Fazekas *et al.*, 1993). Subcortical/deep WMHs were manually labelled on the FLAIR images of each subject using the Display software (McConnell Brain Imaging Centre, MNI, McGill University, Montreal, QC, Canada) and resampled to binary WMH masks. In addition to hemispheric cerebral white matter, the term 'deep' WMHs here included the deep grey matter and brainstem. Periventricular WMHs were not labelled, as the vast majority of subjects displayed only caps, lines or small halos, corresponding to a Fazekas score of 0–2, which reflects disruptions of the ependymal lining with subependymal gliosis and concomitant loss of myelin, but no ischemic pathology (Fazekas *et al.*, 1998).

The diffusion tensor imaging sequence scan was performed using double SE single shot echo-planar imaging with 26 gradient directions ($b = 1000$ s/mm^2) and 6 ($b = 0$ s/mm^2) acquisitions. Diffusion tensor imaging tractography was performed using in-house implementation of the fiber assignment with continuous tracking algorithm (Mori *et al.*, 1999; Mori and van Zijl, 2002) with stopping criteria of fractional anisotropy <0.15 and angle between neighbouring primary diffusion direction $<45°$. Tracking was initiated from the centre of every voxel in the brain. The FLAIR images were registered to the diffusion tensor imaging ($b = 0$) images and the binary WMH masks were applied to identify the fiber tracts intersecting one or more WMHs as described in more detail elsewhere (Dalby *et al.*, 2010*b*; see also illustration in Fig. 1). Subsequently, the WMH masks were excluded from the tract masks to avoid overlapping compartments for perfusions measurements. Segmentation of total white matter was obtained by processing the T1-weigthed images using a standardized pipeline (Aubert-Broche *et al.*, 2013). From this white matter mask the segmented WMHs and tracking masks were subtracted to obtain a mask for NAWM. WMH count, volume and load was calculated in FLAIR image space to avoid artefacts from resampling to T1 space. We compared WMH count, volume and load between groups in the following standard anatomical regions of interest (ROIs): Whole brain; frontal, temporal, parietal and occipital white matter; cerebellum and brainstem. To account for central areas involved in cognition we also included the hippocampus and deep grey matter structures including the thalamus and basal ganglia, the latter subdivided into the caudate nucleus, putamen, globus pallidus and subthalamic nucleus. The substantia nigra and nucleus accumbens were not included in the ROI volumes due to their diminutive size. WMH load was calculated as % WMH volume of the predefined ROI volumes.

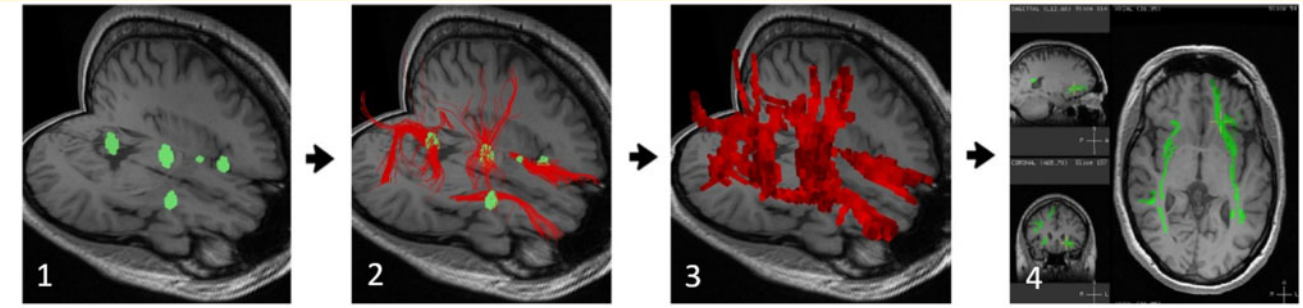

Figure 1 Illustration of tractography procedure. (1) Subcortical/deep WHMs were manually labelled (green) for each subject and dilated one voxel in each direction, here superimposed on a T1-weighted dataset, and saved as binary WMH masks. (2) Tracking was initiated from the centre of every voxel in the brain and as such independent of ROIs. By applying the segmented binary WMH mask to the tractography map for each subject, we identified tracts intersected by one or more WMHs (illustrated by red tracts). (3) The tracts intersected by WMHs were saved as binary tracking masks for each subject, with each voxel assigned a value of 0 (no tract) or 1 (tract intersecting one or more WMHs). For visual purpose the resulting binary tracking mask in this example is labelled red with different colour intensity, reflecting the underlying ** fractional anisotropy FA value range. (4) An example of a binary tracking mask, representing fiber tracts intersected by one or more WMHs, presented as a projection of the 3D tracts onto the subject's own T1-weighted data set. A more detailed description of the procedure is given in Dalby *et al.* (2010*b*).

Perfusion maps

We calculated parametric perfusion maps based on deconvolution of each image voxel's tissue concentration–time curve with the arterial input function (Mouridsen *et al.*, 2006*a*; Mouridsen *et al.*, 2006*b*; Mouridsen *et al.*, 2014). Cerebral blood volume (CBV) in each voxel was determined as the area under the concentration–time curve, while capillary mean transit time (MTT) and capillary transit time heterogeneity (CTH) were determined as the mean and standard deviation of the transit time distributions estimated during the deconvolution procedure. By affecting oxygen extraction efficacy for a given blood supply, CTH acts in concert with CBF to determine net oxygen availability and hence the balance between tissue oxygen metabolism and tissue oxygen tension (P_tO_2) in steady state (Jespersen and Ostergaard, 2012). Thus, for a given tissue P_tO_2, the oxygen extraction fraction (OEF) can be calculated from MTT and CTH (Jespersen and Ostergaard, 2012), and the steady state cerebral metabolic rate of oxygen ($CMRO_2$) under these conditions as OEFxCBF, where CBF is related to MTT through the central volume theorem: CBF = CBV/MTT. CBF was independently estimated in the deconvolution process. The relative transit time heterogeneity (RTH) was calculated as the CTH:MTT ratio. RTH depends on both the topology and hemodynamic functioning of the microvascular bed, both of which may affect oxygen extraction efficacy for a given CBF. Because parametric CBV, CBF and $CMRO_2$ maps are relative rather than absolute, we normalized them (termed nCBV, nCBF and $nCMRO_2$) to whole-brain values by dividing the median values for each ROI with the median value of the whole-brain mask for each subject.

The $CMRO_2$ values calculated above assume a fixed, normal tissue P_tO_2 of 25 mmHg. If local hemodynamics deteriorate, sustained oxygen utilization causes OEF to increase and P_tO_2 to drop, as observed in ischemia and indeed SVD (Meguro *et al.*, 1990; Yamauchi *et al.*, 1991; Yao *et al.*, 1992). To ascertain whether local hemodynamics suffice to support normal tissue metabolism, only at the expense of relative tissue hypoxia, we estimated the resulting P_tO_2 at a normal $CMRO_2$ of 2.5 ml/100 ml/min, derived from quantitative hemispheric positron emission tomography data (Sette *et al.*, 1989). If the P_tO_2 required to achieve this oxygen utilization was low, local hemodynamics was taken to indicate either tissue hypoxia or local hypometabolism. Since SE data more closely reflect capillary hemodynamics than GRE (Boxerman *et al.*, 1995), the $CMRO_2$, OEF and P_tO_2 calculations were performed only for the SE data.

Median values of nCBF, nCBV, MTT, CTH, RTH, $nCMRO_2$, OEF and P_tO_2 (the three latter only for SE data) were extracted from each individual's corresponding parametric maps in (i) total and individual WMHs, (ii) fiber tracts intersected by WMHs and (iii) NAWM. Perfusion data were not obtainable for WMHs localized in close proximity to air-filled sinuses due to image artefacts.

Retinal photography

The retinal and cerebral microvasculature is subjected to similar vascular regulatory processes, including autoregulation (Patton *et al.*, 2005), although retinal vessels lack autonomic innervation (Laties, 1967). Retinal microvascular changes show some associations with cerebral SVD changes, such as WMHs and stroke (Sharrett, 2007), and we therefore obtained retinal photographs to further characterize cerebral microvascular disease changes across subjects and groups. Following administration of tropicamide 1% (Alcon, Rødovre, Denmark) and phenylephrine

10% (SAD, Copenhagen, Denmark) to both eyes, we performed 60° fundus photography using a Canon CF 60Z camera (Canon, Amstelveen, Holland) with one photograph centred on the fovea and another centred on the optic disk (Supplementary Fig. 1). Diapositives were then digitized in 2400 × 2400 dpi resolution using a HP diapositive scanner (Hewlett-Packard, Palo Alto, CA, USA) and analysed in Corel Draw, version 11 (Corel, Maidenhead, UK) at ×64 magnifications by a person (P.J.) blinded to the identity of the study subjects. For each eye, the diameter of the superior and inferior temporal retinal arterioles and venules were measured manually using a built-in ruler. Measurements were conducted as close as possible to the optic disk, while requiring that arteriole and venule are unbranched and clearly separated from other vessels. Finally, for each set of vessels, the ratio between the arteriolar and the venular diameter (the arterio-venous ratio (AV ratio)) was calculated, giving a total of 4 AV ratios per subject, i.e. one superior and inferior AV ratio in each eye, respectively.

Statistical analysis

All statistics were carried out using Stata, release 13 (StataCorp LP, College Station, TX, USA), with two-sided tests and a 5% level of significance. Differences in clinical variables and regional WMH data between groups were assessed with the Wilcoxon two-sample rank-sum test for continuous variables and Fisher's exact test for categorical variables (Table 1 and Supplementary Table 1). With the assumption of a Gaussian distribution of the perfusion parameters, we performed regression analyses to test for group differences, adjusting for various demographic variables, including age, gender, smoking status, tobacco usage in years, hypertension, etc. We pooled patient and control data for further analyses, comparing perfusion parameters in WMHs, tracts and NAWM in paired samples for each individual, e.g. mean CTH in WMHs compared with mean CTH in NAWM, using paired *t*-tests. The Bonferroni correction for multiple comparisons was applied.

Correlations between the number, volume, and perfusion parameters of total and individual WMHs were evaluated by linear regression, the latter with standard error adjusted for clustering.

Differences in retinal vessel diameters and AV ratios between groups were tested with two-sample t-tests with equal variances (Supplementary Table 2). The intraobserver reliability (repeatability) of retinal vessel caliber measurements was tested using Cronbach's α test in 10 randomly chosen subjects in whom the caliber measurement of the superior and inferior temporal retinal arterioles and venules was repeated.

Data availability

Anonymized data may be made available upon reasonable request to the corresponding author.

Results

Table 1 shows clinical data, including total WMH number and volume, for all subjects. Of the originally

Table 1 Clinical data on all subjects

	Patients ($n = 21$)		Controls ($n = 21$)		Statistics	
	Mean	SD	Mean	SD	z	*P*
Age (years)	57.40	4.67	58.49	6.67	0.19	0.85
Tobacco years	22.39	19.52	6.35	9.98	−3.27	0.001*
Vascular risk factor score[a]	7.05	4.73	6.48	4.27	−0.34	0.73
Framingham 10-year stroke risk (%)	6.56	7.26	5.46	5.96	−0.62	0.54
Number of WMHs	19.57	24.77	21.95	28.70	0.88	0.38
Volume of WMHs (mm^3)	791.37	1199.67	1136.59	2154.94	0.92	0.36
Volume of individual WMHs (mm^3)	36.19	45.31	42.84	70.47	1.15	0.25
	n (%)		*n* (%)		*P*	
Gender	–		–		1.00	
Male	7 (33)		7 (33)		–	
Female	14 (67)		14 (67)		–	
Hypertension	7 (33)		5 (24)		0.73	
Smoking	–		–		–	
Current	11 (52)		3 (14)		0.02*	
Past	7 (33)		8 (38)		1.00	
Never	3 (14)		10 (48)		0.04*	
Hypercholesterolemia	8 (38)		9 (43)		1.00	
Diabetes	1 (5)		1 (5)		1.00	
Cardiovascular disease	3 (14)		0 (0)		0.23	

The statistics columns show *P*-values from Mann–Whitney or Fisher's exact tests, respectively.

[a]Composite score as described in the Framingham Study (Wolf *et al.*, 1991), comprising age, systolic blood pressure, antihypertensive treatment, diabetes, cigarette smoking, cardiovascular disease (coronary heart disease, cardiac failure or intermittent claudication), atrial fibrillation and left ventricular hypertrophia.

*$P < 0.05$.

included 22 patients and 22 controls, perfusion data from one patient and one control were uninterpretable due to a technical error, and their imaging data and WMH count, volume and load were therefore excluded from further analyses. Current smoking was overrepresented in the patient group, who also presented with significantly more tobacco years than the control group. However, the composite vascular risk factor scores and calculated 10-year stroke risk were similar between groups.

Five patients and one control had no WMHs. We found no regional differences in the number, volume, or load of WMH between groups, neither in total, nor in any of the predefined ROIs. Regional WMH statistics are shown in Supplementary Table 1. We found no significant difference in the volume of individual WMHs among the two groups. We found a significant positive correlation between each subject's number of WMHs and both the average volume of their individual WMHs ($n = 36$, $t = 7.76$, $P < 0.001$) and their total WMH lesion volume ($n = 42$, $t = 28.23$, $P < 0.001$); i.e. the more lesions, the larger they are. The correlation between total volume of WMHs versus total number of WMHs for each subject is illustrated in Fig. 2.

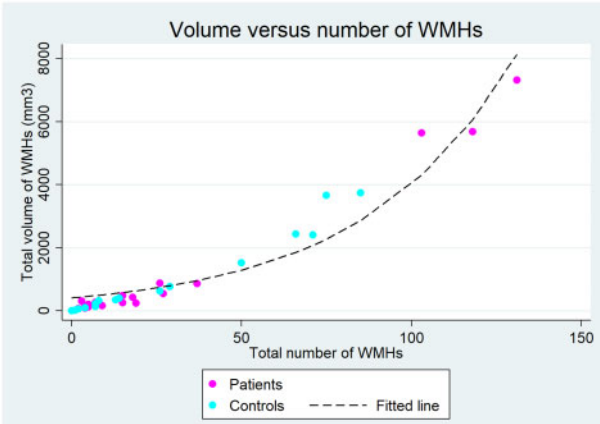

Figure 2 Volume versus number of WMHs. Correlation between total volume of WMHs versus total number of WMHs for each subject (subjects are divided in patients and controls for illustration only). The dashed line represents best fitted function line.

Two of the 21 patients did not complete SE perfusion imaging due to discomfort or technical problems. The total number of subjects for each perfusion analysis is listed in Table 2 (GRE data) and Table 3 (SE data). The left columns of these tables show group-wise comparisons of mean hemodynamic and oxygenation values, adjusted for tobacco usage in years. Regression analyses showed that age, gender, tobacco usage in years, hypertension, diabetes and cardiovascular disease as well as total vascular risk score had a significant effect on several perfusion parameters ($P < 0.05$; results not shown). When adjusting for these possible confounders in the group analyses, only accumulated lifetime smoking, measured as tobacco usage in years, resulted in significant group differences, as shown in Tables 2 and 3 (left). Patients had significantly lower CTH in WMHs for both GRE and SE data ($t = -2.24$; $P = 0.032$ and $t = -2.21$; $P = 0.035$, respectively) than controls, adjusted for tobacco usage in years. Also, we found a significantly higher SE $CMRO_2$ in tracts affected by WMHs ($t = 2.32$; $P = 0.027$) in patients compared with controls, adjusted for tobacco usage in years. However, these differences did not reach significance after application of the Bonferroni correction for multiple comparisons. There were no significant group differences in perfusions parameters when adjusting for any of the other demographic variables ($P > 0.05$; results not shown). Because of the similar distribution of WMHs across the two groups and the lack of differences in perfusion parameters between them, we decided to pool the patient and control data for paired analyses (Tables 2 and 3, right) in accordance with our previous analyses on diffusion data (Dalby *et al.*, 2010*b*). Figure 3 shows bar plots of the means for each parametric map after pooling of the two groups, divided in GRE and SE data. Note the significantly lower nCBF and nCBV and the significantly higher MTT, CTH and RTH in WMHs compared with the fiber tracts they intersect. These differences were found for both GRE and SE data and remained significant after Bonferroni correction for multiple comparisons. Similar findings applied to the perfusion characteristics of WMHs compared with NAWM and tracts intersected by WMHs compared with NAWM, respectively, except for MTT, CTH and RTH, which only applied to WMHs compared with NAWM for SE data after Bonferroni correction (Tables 2 and 3, right). The predicted OEF (SE data only) did not differ between ROIs. Capillary P_tO_2 and $nCMRO_2$ were significantly lower in WMHs compared with both the tracts they intersected and NAWM, but for tracts intersected by WHMs compared with NAWM, only $CMRO_2$ survived the Bonferroni correction (Table 3, right). Figure 4 shows the relation between WMH CBF and P_tO_2, respectively, as a function of the total number and volume of WMHs for each subject. Note, that lower WMH P_tO_2 is associated with both higher WMH number ($n = 34$, $t = -2.13$, $P = 0.041$) and higher total WMH volume ($n = 34$, $t = -2.31$, $P = 0.027$). To examine whether WMH oxygenation could be gleaned from CBF alone, Fig. 5 shows the relation between average (scaled) CBF and P_tO_2 across each subject's WMHs. We observed a positive correlation between CBF and P_tO_2 in individual WMHs ($t = 15.47$, $P < 0.001$) across subjects ($n = 34$). Note, that P_tO_2 values are calculated under the assumption that oxygen is utilized at the rate of normal brain oxygen utilization. The sharp fall in P_tO_2 toward low CBF values thus illustrates how a hypoxic tissue microenvironment is inevitable if tissue metabolism is to be maintained in a state of capillary dysfunction and hypoperfusion.

Table 2 Comparisons between perfusion parameters in WMHs, tracts intersected by WMHs and NAWM for gradient echo data

	Patients				Controls				t	P	Pooled data (n = 36)						t	P
	n	Mean	SD	95% CI	n	Mean	SD	95% CI			n	Mean	SD	95% CI	Comparison	% change		
nCBF																		
(a) WMHs	16	0.52	0.24	0.39–0.64	20	0.51	0.25	0.39–0.63	0.63	0.535	36	0.51	0.24	0.43–0.60	a versus b	−18.1	−3.76	0.0006**
(b) Tracts	16	0.60	0.11	0.54–0.66	20	0.65	0.12	0.59–0.70	−0.37	0.717	36	0.63	0.12	0.59–0.67	a versus c	−29.0	−4.97	0.0000**
(c) NAWM	21	0.71	0.06	0.68–0.74	21	0.72	0.05	0.70–0.74	−1.00	0.326	36	0.72	0.06	0.70–0.73	b versus c	−13.4	−4.84	0.0000**
nCBV																		
(a) WMHs	16	0.57	0.10	0.51–0.62	20	0.57	0.07	0.53–0.60	−0.23	0.817	36	0.57	0.08	0.54–0.59	a versus b	−15.9	−9.98	0.0000**
(b) Tracts	16	0.67	0.08	0.63–0.71	20	0.68	0.05	0.66–0.70	−0.73	0.469	36	0.67	0.06	0.65–0.70	a versus c	−26.6	−14.99	0.0000**
(c) NAWM	21	0.77	0.05	0.75–0.79	21	0.77	0.04	0.75–0.78	−0.64	0.525	36	0.77	0.05	0.75–0.78	b versus c	−12.7	−9.60	0.0000**
MTT																		
(a) WMHs	16	2.31	0.90	1.83–2.79	20	2.37	1.01	1.90–2.85	−2.03	0.051	36	2.34	0.95	2.02–2.67	a versus b	14.0	3.39	0.0018**
(b) Tracts	16	2.17	0.64	1.82–2.51	20	1.97	0.61	1.68–2.25	−0.96	0.346	36	2.06	0.62	1.85–2.27	a versus c	12.6	2.36	0.0238*
(c) NAWM	21	2.29	0.62	2.01–2.57	21	2.05	0.62	1.76–2.33	−0.23	0.820	36	2.08	0.62	1.97–2.36	b versus c	−1.3	−0.65	0.5190
CTH																		
(a) WMHs	16	2.91	1.58	2.07–3.75	20	3.18	1.36	2.54–3.82	−2.24	0.032*	36	3.06	1.45	2.57–3.55	a versus b	17.8	3.19	0.0030**
(b) Tracts	16	2.62	1.15	2.01–3.23	20	2.57	0.88	2.16–2.98	−1.24	0.166	36	2.60	0.99	2.26–2.93	a versus c	18.5	2.68	0.0110*
(c) NAWM	21	2.79	1.09	2.29–3.28	21	2.68	0.86	2.29–3.07	−0.64	0.523	36	2.58	0.93	2.43–3.04	b versus c	0.6	0.21	0.8328
RTH																		
(a) WMHs	16	1.37	0.13	1.30–1.44	20	1.41	0.15	1.34–1.48	−1.41	0.169	36	1.39	0.14	1.34–1.44	a versus b	4.4	3.34	0.0020**
(b) Tracts	16	1.34	0.11	1.28–1.40	20	1.33	0.11	1.28–1.38	0.00	0.996	36	1.33	0.10	1.30–1.37	a versus c	6.4	3.87	0.0004**
(c) NAWM	21	1.33	0.11	1.27–1.38	21	1.31	0.09	1.26–1.35	0.87	0.390	36	1.31	0.10	1.28–1.35	b versus c	1.9	2.85	0.0072*

For the pooled data (patients and controls), the calculated % change in perfusion parameters reflects how adaptation to lower metabolism may affect microcirculation and limit oxygenation. CI = confidence interval; CTH = capillary transit time heterogeneity.

*$P < 0.05$,

**$P \leq 0.003$ (significance level after Bonferroni correction with $\alpha = 0.05$ and 15 tests).

Retinal photography

In three patients and four controls, AV ratios could not be determined for one or more vessel pairs due to insufficient image quality. Supplementary Table 2 shows the distribution of AV ratios across subjects. The intraobserver reliability (repeatability) of retinal vessel caliber measurements was excellent (Cronbach's $\alpha = 0.90$–0.93). No statistically significant differences in vessel diameter or AV ratios were found between groups.

Discussion

This study extends our knowledge on WMHs and WMH pathology in both late-onset depression and normal aging. First, our study showed no evidence of differences between depressed patients and controls in terms of the hemodynamics and oxygenation of their WMHs, the tracts intersected by WMHs or in their NAWM. This applied to both GRE and SE imaging. Taken together with our earlier analyses of WMHs and white matter integrity of the subjects of this study cohort (Dalby *et al.*, 2010*a*, *b*), our data extend earlier studies of WMHs in late onset-depression (Thomas *et al.*, 2002) to suggest that if WMHs confer vulnerability to late-onset depression, this owes to their localization within the frontal white matter circuitry, rather than depression-specific structural or physiological WMH properties.

Second, our study extends earlier observations of reduced capillary density within WMHs as well as NAWM (Brown *et al.*, 2007) by showing that the reduction in capillary density in seemingly unaffected white matter is partly accounted for by its localization within fiber tracts intersected by remote WMHs. This knowledge is obtained by combining SE perfusion imaging, which is sensitized to contrast media in capillary-sized vessels, and outlines of WMHs and the white matter tracts they intersect. Our earlier analyses of these affected fiber tracts revealed microstructural white matter changes suggestive of fiber loss or damage (Dalby *et al.*, 2010*b*), and the reduced CBV and CBF in white matter tracts intersected by WMHs may therefore reflect long-term adaptations to lower white matter oxygen utilization, initiated by remote WMHs. Interestingly, Promjunyakul *et al.* (2016) recently reported diffusion changes as well as reduced CBF in NAWM surrounding WMHs, dubbing this the 'CBF penumbra', and data from the CATCH study (Bernbaum *et al.*, 2015) suggest that reduced CBF in NAWM predicts the development of WMHs. While reduced capillary density, hypoperfusion and capillary dysfunction confer tissue vulnerability in their own right, our findings suggest that fiber tracking may serve as a means of testing whether hypoperfusion owes partly to hypometabolism secondary to remote tissue injury and thus reflects upon existing lesion load. This could be a 'threshold' effect of the hypoxic/ischemic severity of WMHs, causing reduced capillary density in the affected fiber tracts and subsequent hypometabolism and impaired neural transmission.

Third, we found reduced nCBF and nCBV and increased MTT in WMHs compared with NAWM,

Table 3 Comparisons between perfusion parameters in WMHs, tracts intersected by WMHs and NAWM for spin echo data

	Patients				Controls				t	P	Pooled data (n = 36)						t	P
	n	Mean	SD	95% CI	n	Mean	SD	95% CI			n	Mean	SD	95% CI	Comparison	% change		
nCBF																		
(a) WMHs	14	0.55	0.14	0.47–0.63	20	0.48	0.16	0.40–0.55	1.79	0.083	34	0.51	0.15	0.45–0.56	a versus b	−22.8	−8.13	0.0000**
(b) Tracts	14	0.68	0.08	0.63–0.72	20	0.64	0.10	0.60–0.69	1.95	0.061	34	0.66	0.09	0.62–0.69	a versus c	−32.3	−8.80	0.0000**
(c) NAWM	19	0.74	0.09	0.70–0.78	21	0.73	0.06	0.71–0.76	−0.60	0.550	34	0.75	0.07	0.71–0.76	b versus c	−12.4	−5.08	0.0000**
nCBV																		
(a) WMHs	14	0.70	0.09	0.64–0.75	20	0.66	0.12	0.60–0.72	0.63	0.534	34	0.67	0.11	0.64–0.71	a versus b	−10.7	−6.95	0.0000**
(b) Tracts	14	0.77	0.05	0.74–0.80	20	0.75	0.07	0.72–0.78	0.89	0.380	34	0.76	0.06	0.73–0.78	a versus c	−17.6	−7.99	0.0000**
(c) NAWM	19	0.82	0.05	0.79–0.84	21	0.81	0.04	0.79–0.83	−0.83	0.409	34	0.82	0.04	0.80–0.83	b versus c	−7.8	−6.29	0.0000**
MTT																		
(a) WMHs	14	3.05	1.01	2.47–3.63	20	2.98	1.11	2.46–3.50	−1.47	0.153	34	3.01	1.05	2.64–3.38	a versus b	20.1	5.33	0.0000**
(b) Tracts	14	2.66	0.88	2.15–3.17	20	2.40	0.62	2.11–2.69	−0.59	0.561	34	2.51	0.74	2.25–2.76	a versus c	26.2	5.07	0.0000**
(c) NAWM	19	2.57	0.88	2.14–3.00	21	2.31	0.53	2.07–2.55	0.50	0.623	34	2.39	0.71	2.20–2.66	b versus c	5.0	2.18	0.0369*
CTH																		
(a) WMHs	14	3.97	1.95	2.84–5.10	20	4.39	2.19	3.36–5.41	−2.21	0.035*	34	4.22	2.08	3.49–4.94	a versus b	25.6	4.29	0.0001**
(b) Tracts	14	3.32	1.55	2.42–4.21	20	3.39	1.14	2.85–3.92	−1.81	0.080	34	3.36	1.31	2.90–3.81	a versus c	41.3	4.64	0.0001**
(c) NAWM	19	2.83	1.24	2.24–3.43	21	3.22	0.84	2.84–3.60	−1.35	0.184	34	2.98	1.10	2.70–3.37	b versus c	12.5	2.60	0.0140*
RTH																		
(a) WMHs	14	1.53	0.19	1.42–1.64	20	1.49	0.21	1.39–1.59	−0.44	0.665	34	1.51	0.20	1.44–1.58	a versus b	6.8	5.65	0.0000**
(b) Tracts	14	1.45	0.19	1.34–1.56	20	1.39	0.15	1.31–1.46	−0.25	0.805	34	1.41	0.17	1.35–1.47	a versus c	9.8	5.77	0.0000**
(c) NAWM	19	1.41	0.18	1.32–1.50	21	1.34	0.14	1.28–1.40	0.63	0.532	34	1.37	0.17	1.32–1.42	b versus c	2.9	3.05	0.0045*
$nCMRO_2$																		
(a) WMHs	14	0.55	0.13	0.48–0.63	20	0.48	0.13	0.42–0.54	1.88	0.069	34	0.51	0.14	0.46–0.56	a versus b	−22.0	−8.82	0.0000**
(b) Tracts	14	0.67	0.08	0.63–0.72	20	0.64	0.07	0.60–0.67	2.32	0.027*	34	0.65	0.08	0.63–0.68	a versus c	−32.4	−9.97	0.0000**
(c) NAWM	19	0.75	0.09	0.71–0.79	21	0.74	0.06	0.71–0.76	−0.58	0.564	34	0.75	0.07	0.72–0.77	b versus c	−13.4	−6.51	0.0000**
OEF																		
(a) WMHs	14	0.29	0.01	0.28–0.29	20	0.29	0.02	0.28–0.30	−0.93	0.361	34	0.29	0.01	0.28–0.29	a versus b	1.0	1.63	0.1121
(b) Tracts	14	0.29	0.01	0.28–0.29	20	0.29	0.01	0.28–0.29	0.10	0.920	34	0.29	0.01	0.28–0.29	a versus c	0.3	0.41	0.6858
(c) NAWM	19	0.29	0.01	0.28–0.29	21	0.29	0.01	0.29–0.29	0.73	0.469	34	0.29	0.01	0.29–0.29	b versus c	−0.7	−1.34	0.1887
PtO_2																		
(a) WMHs	14	16.98	9.13	11.72–22.25	20	17.96	8.05	14.19–21.73	1.16	0.254	34	17.56	8.39	14.63–20.48	a versus b	−18.1	−5.74	0.0000**
(b) Tracts	14	20.11	7.26	15.92–24.30	20	22.35	5.94	19.58–25.13	0.48	0.631	34	21.43	6.51	19.16–23.70	a versus c	−22.4	−5.48	0.0000**
(c) NAWM	19	20.87	7.16	17.42–24.32	21	23.33	5.17	20.98–25.68	−0.42	0.677	34	22.62	6.28	20.17–24.16	b versus c	−5.3	−2.45	0.0197*

For the pooled data (patients and controls), the calculated % change in perfusion parameters reflects how adaptation to lower metabolism may affect microcirculation and limit oxygenation. CI = confidence interval; CTH = capillary transit time heterogeneity.

*$P < 0.05$,

**$P \leq 0.002$ (significance level after Bonferroni correction with $\alpha = 0.05$ and 24 tests).

consistent with earlier reports (Marstrand *et al.*, 2002; O'Sullivan *et al.*, 2002; Sachdev *et al.*, 2004; Brickman *et al.*, 2009; Uh *et al.*, 2010; Sam *et al.*, 2016). We extended these measurements to address the microvascular distribution of blood in terms of CTH, the standard deviation of their within-voxel transit times. In normal passive, compliant microvascular networks, CTH vary in proportion to MTT (Rasmussen *et al.*, 2015) and increases in the CTH: MTT ratio (i.e. RTH) are therefore thought to reflect abnormal capillary flow patterns, indicative of severe disturbances of capillary morphology and function across tissue microcirculation. Consistent with this notion, we and others have found RTH changes to correlate with disease severity in human conditions known to be associated with microvascular changes, including Alzheimer's disease (Eskildsen *et al.*, 2017; Nielsen *et al.*, 2017), ischemia (Ostergaard *et al.*, 2015; Engedal *et al.*, 2018) and X-linked adrenoleukodystrophy (Lauer *et al.*, 2017). When utilizing perfusion MRI sensitized to capillary-sized vessels, we found RTH to be significantly elevated in both WMHs and in the tracts they intersect when compared with NAWM, although the comparison of tracts to NAWM remained a tendency after adjustment for multiple comparisons. These findings highlight the role of capillaries in the pathophysiology of SVD (Ostergaard *et al.*, 2016) and indicate that a severe microscopic maldistribution of blood exists within white matter affected by WMHs.

Fourth, we assessed the oxygenation resulting from hypoperfusion and microscopic 'shunting' of oxygenated blood (i.e. capillary dysfunction), combined, in terms of (i) the drop in oxygen tension that would result if normal oxygen utilization is preserved and (ii) the drop in oxygen utilization that would result if oxygen tension was maintained at normal brain tissue levels. According to these data, WMHs and affected white matter can only maintain normal white matter oxygen utilization if the OEF is elevated and local oxygen tension thereby reduced. The 22% reduction in P_tO_2, observed on average across our cohort's WMHs compared with NAWM (Table 3, pooled data), would roughly correspond to an increase in OEF from 30% to 50% of blood oxygen

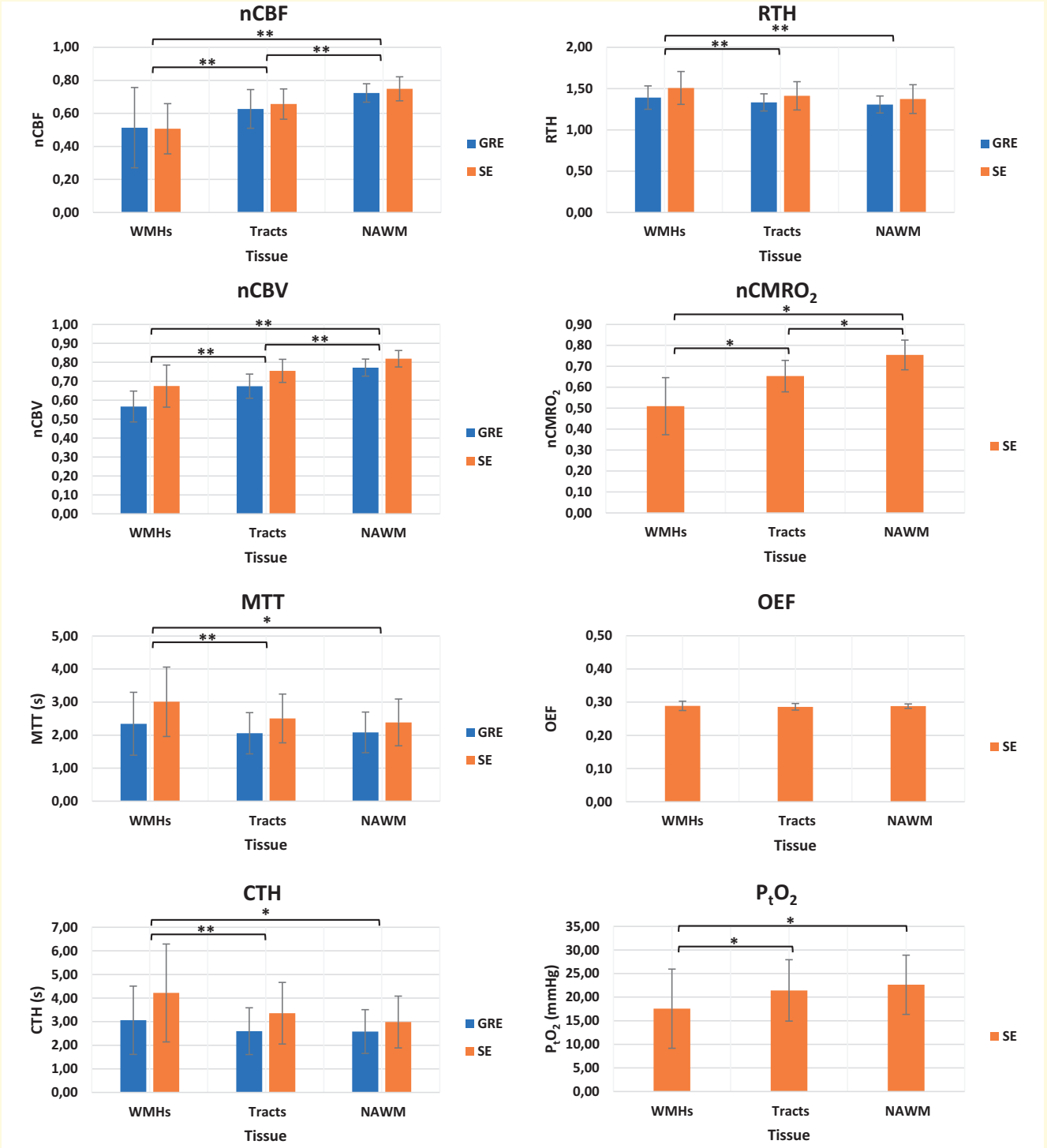

Figure 3 Perfusion values in WMHs, intersected tracts and NAWM. Bar plots of mean perfusion values in WMHs, tracts intersected by WMHs and NAWM for the pooled patient and control groups ($n = 36$). The values for CBF, CBV and $CMRO_2$ are normalized to whole-brain values (termed nCBF, nCBV and $nCMRO_2$, respectively). An asterisk above the horizontal brackets indicates significance for both GRE and SE data at a *P*-value of $\leq$0.003 (GRE data) or $\leq$0.002 (SE data), which is the significance level after Bonferroni correction with $\alpha = 0.05$ and 15 or 24 tests, respectively, as listed in Tables 2 and 3. Two asterisks above the horizontal brackets indicates significance for SE data only, representing a *P*-value of $\leq$0.002, which is the significance level after Bonferroni correction with $\alpha = 0.05$ and 24 tests, as listed in Table 3.

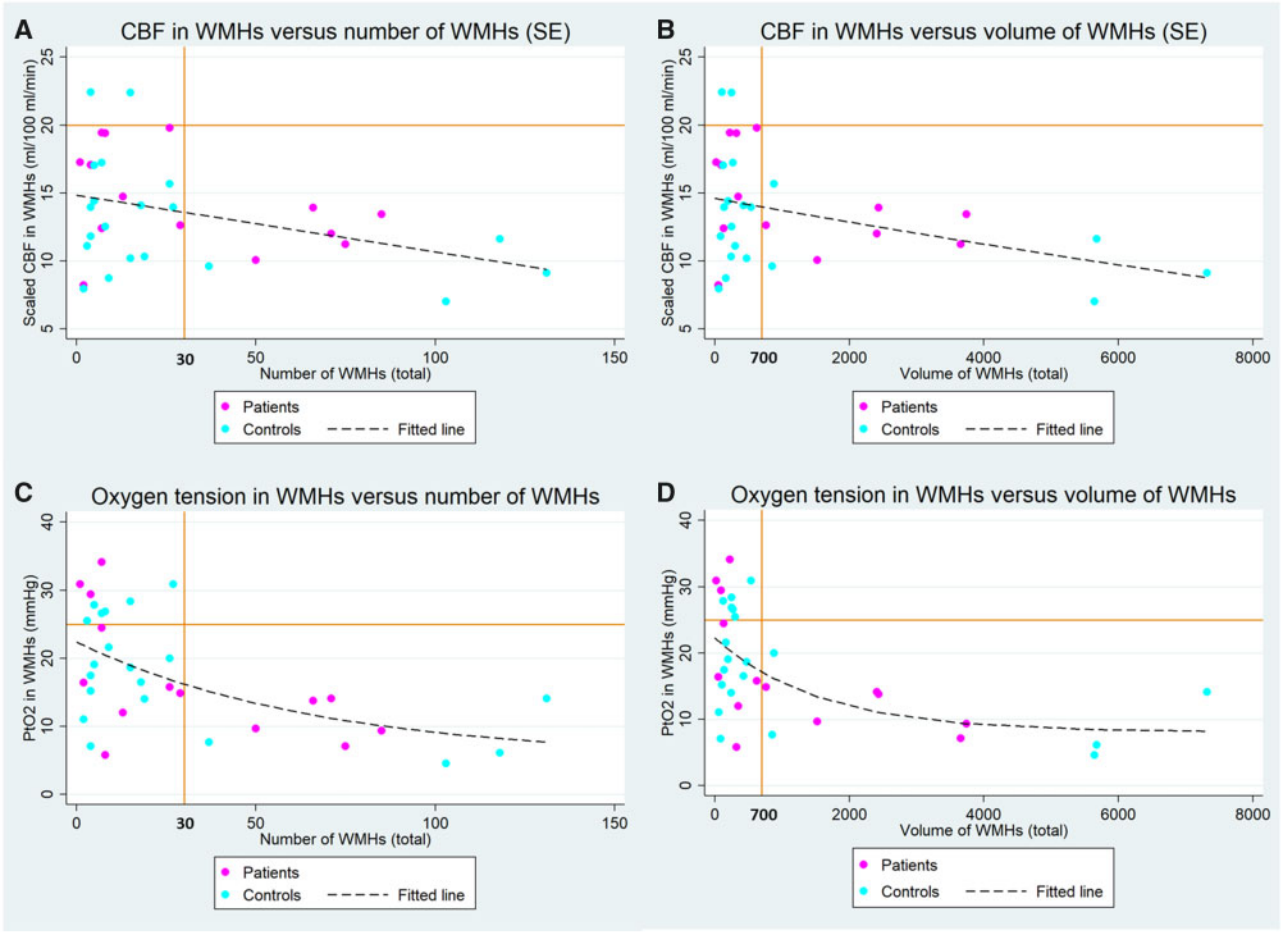

Figure 4 CBF and oxygenation in WMHs versus total number and volume of WMHs. Scatter plots of CBF versus total number (**A**) and total volume (**B**) of WMHs and P_tO_2 versus total number (**C**) and total volume (**D**) of WMHs for each subject, respectively. The CBF values in WMHs in **A** and **B** are scaled after assuming a normal CBF of 20 ml/100 ml/min in NAWM. The horizontal orange line in **A** and **B** indicates this widely accepted normal CBF = 20 ml/100 ml/min of NAWM, whereas the horizontal orange line in **C** and **D** indicates a normal P_tO_2 = 25 mm Hg in NAWM. CBF and P_tO_2 are consistently low when WMHs reach a total number of 30 and a total WMH volume of ~700 mm^3 (vertical orange lines). The dashed lines represent best fitted function lines. The plots represent pooled SE data and are divided in patients and controls for illustration only.

content, that is a 67% OEF increase. In comparison, direct measurements of oxygen utilization by positron emission tomography imaging in SVD patients have shown markedly increased (+30%) OEF and reduced (−22%) CBF, but only slightly reduced oxygen utilization, in the white matter of hypertensive, non-demented subjects with WMHs compared with controls, whereas patients with vascular dementia showed a coupled reduction in white matter CBF and oxygen utilization—that is, only slightly increased OEF (Yao *et al.*, 1992). The resolution of positron emission tomography is inherently low compared with the size of WMHs and individual fiber tracts, so the spatial distribution of oxygen utilization within white matter is difficult to resolve with this gold standard method. Our data suggest, however, that WMHs, with poor oxygenation, but partly preserved oxygen utilization, may contribute to the observed, disproportionate changes in CBF and $CMRO_2$ in the early stages of SVD.

Finally, we found evidence of capillary dysfunction, that is a microscopic maldistribution of blood within WMH image voxels. Capillary dysfunction reduces oxygen availability for a given CBF by allowing oxygenated blood to be 'shunted' through the microcirculation. While capillary dysfunction appears to be a shared feature of SVD and its risk factors (Ostergaard *et al.*, 2016), our results show that WHMs are associated with worse capillary function than surrounding white matter (as detected by RTH) and with severely impaired oxygenation (cf. Fig. 3). Recent studies suggest that reduced oxygenation impairs capillary function, which again impairs tissue oxygenation in a vicious cycle: in a mouse model of chronic hypoperfusion, Srinivasan *et al.* (2015) thus

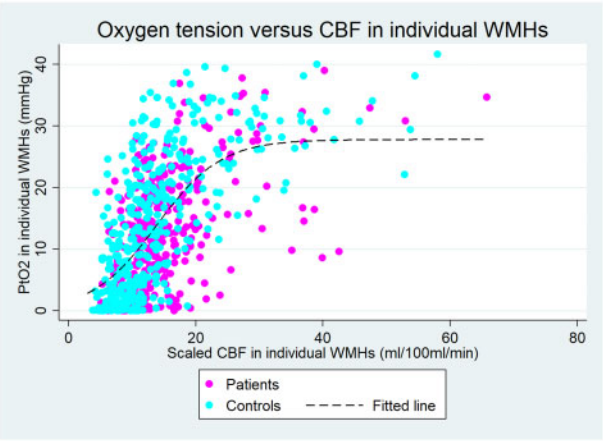

Figure 5 CBF and oxygenation in individual WMHs. Correlation between scaled CBF and P_tO_2 in individual WMHs. NAWM CBF was set to 20 ml/100 ml/min to allow visual comparison of WMH CBF across subjects. The best fitted line approximates a logarithmic function.

found that the density of perfused capillaries decreases in proportion to the reduction in CBF, reaching as many as 25% erythrocyte-free capillaries for blood flows well above the ischemic threshold. In a similar model, Yata *et al.* (2014) detected minute-long plugging of a significant proportion of deep cortical capillaries by leukocytes and ascribed this to adhesion of activated leukocytes to the capillary endothelium via surface receptors (selectins). We note in passing that such disruptions of capillary erythrocyte flow would be expected to introduce capillary dysfunction and impair oxygenation, but not to affect our capillary blood volume estimates, which utilize a tracer that distributes throughout blood plasma. Combined MRI-pathology studies confirm a chronic hypoxic microenvironment within some WMHs (Fernando *et al.*, 2006), and evidence of immune activation and blood-brain barrier dysfunction in others (Rosenberg *et al.*, 2001; Simpson *et al.*, 2007), all of which would be expected to affect capillary function. It is interesting to note that we found capillary density to be reduced to a lesser extent than CBF and $CMRO_2$ within WMHs, seemingly deviating from the normal coupling of capillary density and metabolic demands. We speculate that this finding again reflects the unsuccessful maintenance and/or formation of microvessels to restore supply–demand balance in response to local hypoxia and hypoxia-inducible factor activation (Simpson *et al.*, 2007). The ways in which WMHs interfere with the maintenance of microvascular function are poorly understood, but the lesions are characterized by leakage of plasma fluid components, infiltration and thickening of the arteriolar wall, together with changes in the perivascular tissue, which in turn compromise the normal vascular architecture (Wardlaw *et al.*, 2015). It should also be kept in mind that WMHs are heterogenous, not only in terms of pathology, but also in terms of their evolution over time: Punctate abnormalities on MRI show a low tendency for progression, while early confluent and confluent changes progress more rapidly (Schmidt *et al.*, 2011). The dynamic change in both metabolism and microstructure of cerebral white matter was recently emphasized by Jiaerken *et al.* (2019) with metabolic changes mainly found in NAWM and microstructural changes mainly confined to WMHs. This finding is supported by emerging evidence of cerebral endothelial dysfunction being a pivotal factor in the pathophysiology of cerebral SVD (Ostergaard *et al.*, 2016), and also by studies showing lower vascular reactivity in areas of leukoaraiosis compared with NAWM (Uh *et al.*, 2010; Sam *et al.*, 2016). Unfortunately, due to our cross-sectional study design, the temporal course of capillary dysfunction and neuronal adaptation to underlying microvascular changes remains uncovered.

Reduced CBF, elevated OEF and impaired oxygen utilization are features of cerebral ischemia, and it is therefore tempting to think of WMHs as instances of ischemia or 'misery perfusion', which can be alleviated by improved CBF. It is important to realize, however, that oxygen availability is determined by CBF and capillary function in combination. This notion was recently demonstrated in human stroke, where brain tissue viability during prolonged hypoperfusion was determined not only by CBF alone, as previously believed, but also by RTH (Engedal *et al.*, 2018). The extent to which increased CBF improves tissue oxygenation hinges on the parallel homogenization of capillary flow patterns, and capillary dysfunction may, paradoxically, abrogate the oxygenation benefits of augmenting CBF (Jespersen and Ostergaard, 2012; Angleys *et al.*, 2015). We therefore discourage the use of the term 'ischemia' to characterize tissue hypoxia observed in WMHs, as it implies therapeutic benefits of 'normalizing' CBF. Rather, we propose that tissue oxygenation is determined by CBF and capillary function in combination, and that observations of impaired vascular reactivity in areas of WMHs compared with NAWM (Uh *et al.*, 2010; Sam *et al.*, 2016) should be viewed from the perspective of flow-metabolism coupling, in which flow responses might be attenuated to limit the shunting of oxygenated blood through the microvasculature (Ostergaard *et al.*, 2013*b*). Figure 5 emphasizes the benefits of including not only CBF but also P_tO_2 estimates based on both CBF and CTH, when evaluating the severity of hemodynamic changes in individual WMHs. However, perfusion MRI may not be available in a routine clinical setting. Still, as shown in Fig. 4, the scaled median CBF for each individual's total WMH burden is consistently low (<15 ml/100 ml/min) when the total number of WMHs reaches ~30 and the total volume of WMHs reaches ~700 mm^3. Simplified, and with respect to scaled/normalized perfusion values, this implies that multiple and/or large WMHs reflect a chronic hypoxic environment, consistent with the concept of WMHs of

presumed vascular origin, presented as a part of the neuroimaging standards in SVD research (Wardlaw *et al.*, 2013).

Retinal photography

We used retinal photography to calculate retinal AV ratios (Supplementary Table 2) as a surrogate marker of cerebral small-vessel disease (Sharrett, 2007). Arteriolar narrowing, small AV ratios and/or AV nicking are often considered markers of long-term hypertension (Wong *et al.*, 2001), which was equally present in our patients and controls (Table 1). However, a small AV ratio can result from both arteriolar narrowing and/or venular enlargement, and the association may vary with age (Sharrett, 2007). We found a tendency ($P = 0.05$) for retinal venular enlargement in the right inferior venules (Supplementary Table 2). As retinal venular enlargement is associated with smoking and inflammation (Ikram *et al.*, 2004) and may reflect lower cerebral oxygen supply (de Jong *et al.*, 2008), we speculate that the higher prevalence of current smokers could favor venous enlargement in our patient group. Although retinal venular enlargement has been associated with progression of cerebral SVD (Ikram *et al.*, 2006*b*) and an increased risk of stroke (Ikram *et al.*, 2006*a*), vascular dementia (de Jong *et al.*, 2011) and schizophrenia (Meier *et al.*, 2013), retinal vessel diameters have not been shown to predict higher risk of depression (Ikram *et al.*, 2010). Overall, the present retinal data give us no basis to suspect that our depressed patients have more pronounced cerebrovascular disease in general than the control group.

Methodological considerations

A major strength of our study is the similar vascular risk profile in patients and controls, except for current smoking, which was more abundant among patients. In addition, retinal AV ratios and the overall white matter lesion load, i.e. count, volume and % of WMHs in predefined ROIs, were similar between groups, thus diminishing the possible confounding effect from an unequal distribution of known markers of microvascular disease. Another strength of our study is the combination of diffusion tensor imaging tractography with dynamic susceptibility contrast perfusion MRI, which enabled us to define tracts intersected by WMHs, not otherwise distinguishable from NAWM.

A limitation of our study is the relatively small sample size regarding both patients and controls, and similar analyses in larger samples are warranted to diminish the risk of type 2 statistical errors. We only included subcortical/deep WMHs in our analyses, thus omitting periventricular WMHs. This distinction between subcortical/deep and periventricular WMHs is debatable (Wardlaw *et al.*, 2013). Our population had very sparse periventricular white matter changes, mostly confined to caps, lines and small halos according to Fazekas' scale (Fazekas *et al.*, 1987) (results not shown). In some literature, these are believed to represent disruption of the ependymal lining of the lateral ventricles, subependymal gliosis and demyelination of non-vascular/non-ischemic origin (Kim *et al.*, 2008; Schmidt *et al.*, 2011). In addition, previous studies have demonstrated both neuropathological (Fazekas *et al.*, 1993; Thomas *et al.*, 2002; Thomas *et al.*, 2003) and functional differences (Kim *et al.*, 2008) between subcortical/deep and periventricular WMHs. Some studies even indicate that subcortical/deep WMHs are more strongly associated with depression than periventricular WMHs (Krishnan *et al.*, 2006; Saavedra Perez *et al.*, 2013). Our conclusions regarding WMHs therefore only apply to subcortical/deep WMHs, but not periventricular WMHs.

We calculated a WMH load as % WMH volume of the predefined ROI volumes for each subject and did not find any difference between patients and controls (Supplementary Table 1). We expect the ROI volumes to reflect intracranial volume, but although the total volume of WHMs is infinitesimal compared with the whole brain volume, the total WMH volume may vary with head size which—in theory—is a source of systematic error.

For ethical reasons, our depressed patients were not treatment-naïve at inclusion, as they all—except for one—received antidepressant medication (Dalby *et al.*, 2010*a*). WMHs have been shown to increase with antidepressant treatment (Steffens *et al.*, 2008; Grool *et al.*, 2013; Khalaf *et al.*, 2015), but the association may be confounded by several factors, such as type of antidepressant, early- or late-onset of depression, remission status and concomitant use of anti-inflammatory medication (Khalaf *et al.*, 2015). The bidirectional relationship of depression and white matter changes is a cornerstone of the vascular depression hypothesis (Alexopoulos *et al.*, 1997; Krishnan *et al.*, 1997), but the complexity of this association is still incompletely understood (Teper and O'brien, 2008). Nevertheless, our data do not indicate a different vascular pathological basis for WMHs between groups.

Finally, our study design is cross-sectional, which prevents us from distinguishing early-stage white matter changes from chronic tissue damage. Prospective studies containing measures of capillary function should further explore the relation between white matter hemodynamics and the emergence of WMHs.

Supplementary material

Supplementary material is available at *Brain Communications* online.

Acknowledgement

The authors wish to thank Mikkel Bo Hansen, CFIN/MINDLab, Aarhus University Hospital, Aarhus, Denmark,

for his contribution to the method development regarding the capillary dysfunction hypothesis.

Funding

Dr. L.Ø. has received funding by the Danish Ministry of Science, Technology and Innovation (grant agreement no. 09-065250) through the MINDLab UNIK initiative at Aarhus University and the Lundbeck Foundation (grant agreement no. R207-2015-1981). Dr. P.V. has received funding by the Danish Council for Independent Research | Medical Sciences (grant agreement no. 271-05-0211). The contrast agent Gadovist® 1.0 M was sponsored by Bayer AG (Berlin, Germany), formerly Schering AG (Berlin, Germany). No pharmaceutical companies, including the supplier of contrast agent, other private or public enterprises, and none of the grant contributors were involved in the design, organization, analysis or preparation for publication of the study.

Competing interests

The authors report no competing interests.

References

Alexopoulos GS, Meyers BS, Young RC, Campbell S, Silbersweig D, Charlson M. 'Vascular depression' hypothesis. Arch Gen Psychiatry 1997; 54: 915–22.

American Psychiatric Association. Diagnostic and statistical manual of mental disorders. 4th edn. Washington, DC: American Psychiatric Association; 2000.

Angleys H, Ostergaard L, Jespersen SN. The effects of capillary transit time heterogeneity (CTH) on brain oxygenation. J Cereb Blood Flow Metab 2015; 35: 806–17.

Aubert-Broche B, Fonov VS, Garcia-Lorenzo D, Mouiha A, Guizard N, Coupe P. A new method for structural volume analysis of longitudinal brain MRI data and its application in studying the growth trajectories of anatomical brain structures in childhood. Neuroimage 2013; 82: 393–402.

Bastin ME, Clayden JD, Pattie A, Gerrish IF, Wardlaw JM, Deary IJ. Diffusion tensor and magnetization transfer MRI measurements of periventricular white matter hyperintensities in old age. Neurobiol Aging 2009; 30: 125–36.

Bernbaum M, Menon BK, Fick G, Smith EE, Goyal M, Frayne R, et al. Reduced blood flow in normal white matter predicts development of leukoaraiosis. J Cereb Blood Flow Metab 2015; 35: 1610–5.

Borowsky IW, Collins RC. Metabolic anatomy of brain: a comparison of regional capillary density, glucose metabolism, and enzyme activities. J Comp Neurol 1989; 288: 401–13.

Boxerman JL, Hamberg LM, Rosen BR, Weisskoff RM. MR contrast due to intravascular magnetic susceptibility perturbations. Magn Reson Med 1995; 34: 555–66.

Brickman AM, Zahra A, Muraskin J, Steffener J, Holland CM, Habeck C, et al. Reduction in cerebral blood flow in areas appearing as white matter hyperintensities on magnetic resonance imaging. Psychiatry Res 2009; 172: 117–20.

Brown WR, Moody DM, Thore CR, Challa VR, Anstrom JA. Vascular dementia in leukoaraiosis may be a consequence of capillary loss not only in the lesions, but in normal-appearing white matter and cortex as well. J Neurol Sci 2007; 257: 62–6.

Brown WR, Thore CR. Review: cerebral microvascular pathology in ageing and neurodegeneration. Neuropathol Appl Neurobiol 2011; 37: 56–74.

Chen PS, McQuoid DR, Payne ME, Steffens DC. White matter and subcortical gray matter lesion volume changes and late-life depression outcome: a 4-year magnetic resonance imaging study. IPG 2006; 18: 445–56.

Dalby RB, Chakravarty MM, Ahdidan J, Sorensen L, Frandsen J, Jonsdottir KY, et al. Localization of white-matter lesions and effect of vascular risk factors in late-onset major depression. Psychol Med 2010a; 40: 1389–99.

Dalby RB, Frandsen J, Chakravarty MM, Ahdidan J, Sorensen L, Rosenberg R, et al. Depression severity is correlated to the integrity of white matter fiber tracts in late-onset major depression. Psychiatry Res 2010b; 184: 38–48.

de Groot M, Verhaaren BF, de Boer R, Klein S, Hofman A, van der Lugt A, et al. Changes in normal-appearing white matter precede development of white matter lesions. Stroke 2013; 44: 1037–42.

de Jong FJ, Schrijvers EM, Ikram MK, Koudstaal PJ, de Jong PT, Hofman A, et al. Retinal vascular caliber and risk of dementia: the Rotterdam study. Neurology 2011; 76: 816–21.

de Jong FJ, Vernooij MW, Ikram MK, Ikram MA, Hofman A, Krestin GP, et al. Arteriolar oxygen saturation, cerebral blood flow, and retinal vessel diameters. The Rotterdam Study. Ophthalmology 2008; 115: 887–92.

de Leeuw FE, de Groot JC, Achten E, Oudkerk M, Ramos LM, Heijboer R, et al. Prevalence of cerebral white matter lesions in elderly people: a population based magnetic resonance imaging study. The Rotterdam Scan Study. J Neurol Neurosurg Psychiatry 2001; 70: 9–14.

Debette S, Markus HS. The clinical importance of white matter hyperintensities on brain magnetic resonance imaging: systematic review and meta-analysis. BMJ 2010; 341: c3666.

Engedal TS, Hjort N, Hougaard KD, Simonsen CZ, Andersen G, Mikkelsen IK, et al. Transit time homogenization in ischemic stroke—a novel biomarker of penumbral microvascular failure? J Cereb Blood Flow Metab 2018; 38: 2006–20.

Eskildsen SF, Gyldensted L, Nagenthiraja K, Nielsen RB, Hansen MB, Dalby RB, et al. Increased cortical capillary transit time heterogeneity in Alzheimer's disease: a DSC-MRI perfusion study. Neurobiol Aging 2017; 50: 107–18.

Fazekas F, Chawluk JB, Alavi A, Hurtig HI, Zimmerman RA. MR signal abnormalities at 1.5 T in Alzheimer's dementia and normal aging. Am J Roentgenol 1987; 149: 351–6.

Fazekas F, Kleinert R, Offenbacher H, Schmidt R, Kleinert G, Payer F, et al. Pathologic correlates of incidental MRI white matter signal hyperintensities. Neurology 1993; 43: 1683–9.

Fazekas F, Ropele S, Enzinger C, Gorani F, Seewann A, Petrovic K, et al. MTI of white matter hyperintensities. Brain 2005; 128: 2926–32.

Fazekas F, Schmidt R, Scheltens P. Pathophysiologic mechanisms in the development of age-related white matter changes of the brain. Dement Geriatr Cogn Disord 1998; 9 Suppl 1: 2–5.

Fernando MS, Ince PG. Vascular pathologies and cognition in a population-based cohort of elderly people. J Neurol Sci 2004; 226: 13–7.

Fernando MS, Simpson JE, Matthews F, Brayne C, Lewis CE, Barber R, et al. White matter lesions in an unselected cohort of the elderly: molecular pathology suggests origin from chronic hypoperfusion injury. Stroke 2006; 37: 1391–8.

Grool AM, Graaf Y, Vincken KL, Witkamp TD, Mali WPTM, Geerlings MI. Antidepressant use is related to larger white matter lesion volume in patients with symptomatic atherosclerotic disease: the SMART-MR study. J Neurol 2013; 260: 197–206.

Herrmann LL, Le MM, Ebmeier KP. White matter hyperintensities in late life depression: a systematic review. J Neurol Neurosurg Psychiatry 2007; 79: 619–24.

Hickie I, Scott E, Mitchell P, Wilhelm K, Austin MP, Bennett B. Subcortical hyperintensities on magnetic resonance imaging: clinical correlates and prognostic significance in patients with severe depression. Biol Psychiatry 1995; 37: 151–60.

Iadecola C. Neurovascular regulation in the normal brain and in Alzheimer's disease. Nat Rev Neurosci 2004; 5: 347–60.

Iadecola C. The pathobiology of vascular dementia. Neuron 2013; 80: 844–66.

Ikram MK, de Jong FJ, Bos MJ, Vingerling JR, Hofman A, Koudstaal PJ, et al. Retinal vessel diameters and risk of stroke: the Rotterdam study. Neurology 2006; 66: 1339–43.

Ikram MK, de Jong FJ, van Dijk EJ, Prins ND, Hofman A, Breteler MM, et al. Retinal vessel diameters and cerebral small vessel disease: the Rotterdam Scan Study. Brain 2006; 129: 182–8.

Ikram MK, de Jong FJ, Vingerling JR, Witteman JC, Hofman A, Breteler MM, et al. Are retinal arteriolar or venular diameters associated with markers for cardiovascular disorders? The Rotterdam Study. Invest Ophthalmol Vis Sci 2004; 45: 2129–34.

Ikram MK, Luijendijk HJ, Hofman A, de Jong PT, Breteler MM, Vingerling JR, et al. Retinal vascular calibers and risk of late-life depression: the Rotterdam study. Am J Geriatr Psychiatry 2010; 18: 452–5.

Iosifescu DV, Renshaw PF, Lyoo IK, Lee HK, Perlis RH, Papakostas GI, et al. Brain white-matter hyperintensities and treatment outcome in major depressive disorder. Br J Psychiatry 2006; 188: 180–5.

Jespersen SN, Ostergaard L. The roles of cerebral blood flow, capillary transit time heterogeneity, and oxygen tension in brain oxygenation and metabolism. J Cereb Blood Flow Metab 2012; 32: 264–77.

Jiaerken Y, Luo X, Yu X, Huang P, Xu X, Zhang M, et al. Microstructural and metabolic changes in the longitudinal progression of white matter hyperintensities. J Cereb Blood Flow Metab 2019; 39: 1613–22.

Khalaf A, Edelman K, Tudorascu D, Andreescu C, Reynolds CF, Aizenstein H. White matter hyperintensity accumulation during treatment of late-life depression. Neuropsychopharmacol 2015; 40: 3027–35.

Kim KW, MacFall JR, Payne ME. Classification of white matter lesions on magnetic resonance imaging in elderly persons. Biol Psychiatry 2008; 64: 273–80.

Klein B, Kuschinsky W, Schrock H, Vetterlein F. Interdependency of local capillary density, blood flow, and metabolism in rat brains. Am J Physiol 1986; 251: H1333–H40.

Kohler S, Thomas AJ, Lloyd A, Barber R, Almeida OP, O'brien JT. White matter hyperintensities, cortisol levels, brain atrophy and continuing cognitive deficits in late-life depression. Br J Psychiatry 2010; 196: 143–9.

Krishnan KR, Hays JC, Blazer DG. MRI-defined vascular depression. Am J Psychiatry 1997; 154: 497–501.

Krishnan MS, O'brien JT, Firbank MJ, Pantoni L, Carlucci G, Erkinjuntti T, et al. Relationship between periventricular and deep white matter lesions and depressive symptoms in older people. The LADIS study. Int J Geriat Psychiatry 2006; 21: 983–9.

Laties AM. Central retinal artery innervation. Absence of adrenergic innervation to the intraocular branches. Arch Ophthalmol 1967; 77: 405–9.

Lauer A, Da X, Hansen MB, Boulouis G, Ou Y, Cai X, et al. ABCD1 dysfunction alters white matter microvascular perfusion. Brain 2017; 140: 3139–52.

Longstreth WT, Jr., Manolio TA, Arnold A, Burke GL, Bryan N, Jungreis CA, et al. Clinical correlates of white matter findings on cranial magnetic resonance imaging of 3301 elderly people. The Cardiovascular Health Study. Stroke 1996; 27: 1274–82.

Maillard P, Fletcher E, Harvey D, Carmichael O, Reed B, Mungas D, et al. White matter hyperintensity penumbra. Stroke 2011; 42: 1917–22.

Maniega SM, Valdes Hernandez MC, Clayden JD, Royle NA, Murray C, Morris Z, et al. White matter hyperintensities and normal-appearing white matter integrity in the aging brain. Neurobiol Aging 2015; 36: 909–18.

Markham JA, Greenough WT. Experience-driven brain plasticity: beyond the synapse. Neuron Glia Biol 2004; 1: 351–63.

Markus HS, Lythgoe DJ, Ostegaard L, O'Sullivan M, Williams SC. Reduced cerebral blood flow in white matter in ischaemic leukoaraiosis demonstrated using quantitative exogenous contrast based perfusion MRI. J Neurol Neurosurg Psychiatry 2000; 69: 48–53.

Marstrand JR, Garde E, Rostrup E, Ring P, Rosenbaum S, Mortensen EL, et al. Cerebral perfusion and cerebrovascular reactivity are reduced in white matter hyperintensities. Stroke 2002; 33: 972–6.

Meguro K, Hatazawa J, Yamaguchi T, Itoh M, Matsuzawa T, Ono S, et al. Cerebral circulation and oxygen metabolism associated with subclinical periventricular hyperintensity as shown by magnetic resonance imaging. Ann Neurol 1990; 28: 378–83.

Meier MH, Shalev I, Moffitt TE, Kapur S, Keefe RS, Wong TY, et al. Microvascular abnormality in schizophrenia as shown by retinal imaging. AJP 2013; 170: 1451–9.

Mori S, Crain BJ, Chacko VP, van Zijl PC. Three-dimensional tracking of axonal projections in the brain by magnetic resonance imaging. Ann Neurol 1999; 45: 265–9.

Mori S, van Zijl PC. Fiber tracking: principles and strategies—a technical review. NMR Biomed 2002; 15: 468–80.

Mouridsen K, Christensen S, Gyldensted L, Ostergaard L. Automatic selection of arterial input function using cluster analysis. Magn Reson Med 2006; 55: 524–31.

Mouridsen K, Friston K, Hjort N, Gyldensted L, Ostergaard L, Kiebel S. Bayesian estimation of cerebral perfusion using a physiological model of microvasculature. Neuroimage 2006; 33: 570–9.

Mouridsen K, Hansen MB, Ostergaard L, Jespersen SN. Reliable estimation of capillary transit time distributions using DSC-MRI. J Cereb Blood Flow Metab 2014; 34: 1511–21.

Nielsen RB, Egefjord L, Angleys H, Mouridsen K, Gejl M, Moller A, et al. Capillary dysfunction is associated with symptom severity and neurodegeneration in Alzheimer's disease. Alzheimers Dement 2017; 13: 1143–53.

O'Sullivan M, Lythgoe DJ, Pereira AC, Summers PE, Jarosz JM, Williams SC, et al. Patterns of cerebral blood flow reduction in patients with ischemic leukoaraiosis. Neurology 2002; 59: 321–6.

Ostergaard L, Engedal TS, Moreton F, Hansen MB, Wardlaw JM, Dalkara T, et al. Cerebral small vessel disease: Capillary pathways to stroke and cognitive decline. J Cereb Blood Flow Metab 2016; 36: 302–25.

Ostergaard L, Jespersen SN, Engedahl T, Gutierrez JE, Ashkanian M, Hansen MB, et al. Capillary dysfunction: its detection and causative role in dementias and stroke. Curr Neurol Neurosci Rep 2015; 15: 37.

Ostergaard L, Aamand R, Gutierrez-Jimenez E, Ho YC, Blicher JU, Madsen SM, et al. The capillary dysfunction hypothesis of Alzheimer's disease. Neurobiol Aging 2013a; 34: 1018–31.

Ostergaard L, Aamand R, Karabegovic S, Tietze A, Blicher JU, Mikkelsen IK, et al. The role of the microcirculation in delayed cerebral ischemia and chronic degenerative changes after subarachnoid hemorrhage. J Cereb Blood Flow Metab 2013b; 33: 1825–37.

Pantoni L. Cerebral small vessel disease: from pathogenesis and clinical characteristics to therapeutic challenges. Lancet Neurol 2010; 9: 689–701.

Pantoni L, Garcia JH. Pathogenesis of leukoaraiosis: a review. Stroke 1997; 28: 652–9.

Patton N, Aslam T, Macgillivray T, Pattie A, Deary IJ, Dhillon B. Retinal vascular image analysis as a potential screening tool for cerebrovascular disease: a rationale based on homology between cerebral and retinal microvasculatures. J Anatomy 2005; 206: 319–48.

Prins ND, Scheltens P. White matter hyperintensities, cognitive impairment and dementia: an update. Nat Rev Neurol 2015; 11: 157–65.

Promjunyakul NO, Lahna DL, Kaye JA, Dodge HH, Erten-Lyons D, Rooney WD, et al. Comparison of cerebral blood flow and structural penumbras in relation to white matter hyperintensities: A multi-modal magnetic resonance imaging study. J Cereb Blood Flow Metab 2016; 36: 1528–36.

Rasmussen PM, Jespersen SN, Ostergaard L. The effects of transit time heterogeneity on brain oxygenation during rest and functional activation. J Cereb Blood Flow Metab 2015; 35: 432–42.

Renkin EBW. Zweifach Award lecture. Regulation of the microcirculation. Microvasc Res 1985; 30: 251–63.

Rosenberg GA, Sullivan N, Esiri MM. White matter damage is associated with matrix metalloproteinases in vascular dementia. Stroke 2001; 32: 1162–8.

Sachdev P, Wen W, Shnier R, Brodaty H. Cerebral blood volume in T2-weighted white matter hyperintensities using exogenous contrast based perfusion MRI. J Neuropsychiatry Clin Neurosci 2004; 16: 83–92.

Sam K, Crawley AP, Poublanc J, Conklin J, Sobczyk O, Mandell DM, et al. Vascular Dysfunction in Leukoaraiosis. AJNR Am J Neuroradiol 2016; 37: 2258–64.

Schmidt R, Schmidt H, Haybaeck J, Loitfelder M, Weis S, Cavalieri M, et al. Heterogeneity in age-related white matter changes. Acta Neuropathol 2011; 122: 171–85.

Sette G, Baron JC, Mazoyer B, Levasseur M, Pappata S, Crouzel C. Local brain haemodynamics and oxygen metabolism in cerebrovascular disease. Positron emission tomography. Brain 1989; 112: 931–51.

Sharrett AR. A review of population-based retinal studies of the microvascular contribution to cerebrovascular diseases. Ophthalmic Epidemiol 2007; 14: 238–42.

Sheline YI, Pieper CF, Barch DM, Welsh-Boehmer K, McKinstry RC, MacFall JR, et al. Support for the vascular depression hypothesis in late-life depression: results of a 2-site, prospective, antidepressant treatment trial. Arch Gen Psychiatry 2010; 67: 277–85.

Simpson JE, Fernando MS, Clark L, Ince PG, Matthews F, Forster G, et al. White matter lesions in an unselected cohort of the elderly: astrocytic, microglial and oligodendrocyte precursor cell responses. Neuropathol Appl Neurobiol 2007; 33: 410–9.

Srinivasan VJ, Yu E, Radhakrishnan H, Can A, Climov M, Leahy C, et al. Micro-heterogeneity of flow in a mouse model of chronic cerebral hypoperfusion revealed by longitudinal Doppler optical coherence tomography and angiography. J Cereb Blood Flow Metab 2015; 35: 1552–60.

Steffens DC, Chung H, Krishnan KR, Longstreth WT, Jr., Carlson M, Burke GL. Antidepressant treatment and worsening white matter on serial cranial magnetic resonance imaging in the elderly: the Cardiovascular Health Study. Stroke 2008; 39: 857–62.

Steffens DC, Conway CR, Dombeck CB, Wagner HR, Tupler LA, Weiner RD. Severity of subcortical gray matter hyperintensity predicts ECT response in geriatric depression. J Ect 2001; 17: 45–9.

Steffens DC, Potter GG, McQuoid DR, MacFall JR, Payne ME, Burke JR, et al. Longitudinal magnetic resonance imaging vascular changes, apolipoprotein E genotype, and development of dementia in the neurocognitive outcomes of depression in the elderly study. Am J Geriatr Psychiatry 2007; 15: 839–49.

Saavedra Perez HC, Direk N, Hofman A, Vernooij MW, Tiemeier H, Ikram MA. Silent brain infarcts: a cause of depression in the elderly?. Psychiatry Res 2013; 211: 180–2.

Taylor WD, Steffens DC, MacFall JR, McQuoid DR, Payne ME, Provenzale JM, et al. White matter hyperintensity progression and late-life depression outcomes. Arch Gen Psychiatry 2003; 60: 1090–6.

Teper E, O'brien JT. Vascular factors and depression. Int J Geriat Psychiatry 2008; 23: 993–1000.

Thomas AJ, O'brien JT, Barber R, McMeekin W, Perry R. A neuropathological study of periventricular white matter hyperintensities in major depression. J Affect Disord 2003; 76: 49–54.

Thomas AJ, O'brien JT, Davis S, Ballard C, Barber R, Kalaria RN, et al. Ischemic basis for deep white matter hyperintensities in major depression: a neuropathological study. Arch Gen Psychiatry 2002; 59: 785–92.

Uh J, Yezhuvath U, Cheng Y, Lu H. In vivo vascular hallmarks of diffuse leukoaraiosis. J Magn Reson Imaging 2010; 32: 184–90.

van Agtmaal MJM, Houben A, Pouwer F, Stehouwer CDA, Schram MT. Association of Microvascular Dysfunction With Late-Life Depression: A Systematic Review and Meta-analysis. JAMA Psychiatry 2017; 74: 729–39.

Wardlaw JM, Smith EE, Biessels GJ, Cordonnier C, Fazekas F, Frayne R, et al. Neuroimaging standards for research into small vessel disease and its contribution to ageing and neurodegeneration. Lancet Neurol 2013; 12: 822–38.

Wardlaw JM, Valdes Hernandez MC, Munoz-Maniega S. What are white matter hyperintensities made of? Relevance to vascular cognitive impairment. J Am Heart Assoc 2015; 4: 001140.

Wolf PA, D'Agostino RB, Belanger AJ, Kannel WB. Probability of stroke: a risk profile from the Framingham Study. Stroke 1991; 22: 312–8.

Wong TY, Klein R, Klein BE, Tielsch JM, Hubbard L, Nieto FJ. Retinal microvascular abnormalities and their relationship with hypertension, cardiovascular disease, and mortality. Surv Ophthalmol 2001; 46: 59–80.

World Health Organization. The ICD-10 classification of mental and behavioural disorders. Diagnostic criteria for research. Geneva: World Health Organization; 1993.

World Medical Association. Declaration of Helsinki. Helsinki: World Medical Association; 2008.

Yamauchi H, Fukuyama H, Yamaguchi S, Miyoshi T, Kimura J, Konishi J. High-intensity area in the deep white matter indicating hemodynamic compromise in internal carotid artery occlusive disorders. Arch Neurol 1991; 48: 1067–71.

Yao H, Sadoshima S, Ibayashi S, Kuwabara Y, Ichiya Y, Fujishima M. Leukoaraiosis and dementia in hypertensive patients. Stroke 1992; 23: 1673–7.

Yata K, Nishimura Y, Unekawa M, Tomita Y, Suzuki N, Tanaka T, et al. In vivo imaging of the mouse neurovascular unit under chronic cerebral hypoperfusion. Stroke 2014; 45: 3698–703.

Zhao T, Zhang CP, Liu ZH, Wu LY, Huang X, Wu HT, et al. Hypoxia-driven proliferation of embryonic neural stem/progenitor cells–role of hypoxia-inducible transcription factor-1alpha. FEBS J 2008; 275: 1824–34.